



# Characterization of the local brittle layer formed in electro-gas weld metals

Kangmyung Seo<sup>1</sup> · Hoisoo Ryoo<sup>2</sup> · Hee Jin Kim<sup>3</sup> · Joong Geun Yoon<sup>3</sup> · Changhee Lee<sup>1</sup>

Received: 10 August 2020 / Accepted: 9 November 2020 / Published online: 14 November 2020  
© International Institute of Welding 2020

## Abstract

The microstructural characteristics of the local brittle layer (LBL) reported to be formed at the weld center of tandem electro-gas (EG) weld made with EG70T-G wire have been investigated to identify the critical factors causing its brittleness and thus facilitate the development of welds free from the local brittle layer. The results showed that in addition to the directional characteristics of columnar grain structures, the proportion of grain boundary ferrite played an important role in LBL formation and in controlling the impact toughness of electro-gas welds at the weld center. These results led to investigate the additional electro-gas welds containing less amounts of grain boundary ferrite with an aim to improve the toughness at weld center. In addition, the relative brittleness of the local brittle layer was evaluated in terms of Charpy V-notch ductile-brittle transition curves and a stepwise transition unusually obtained from local brittle layer was discussed from the perspective of the microstructural characteristics of LBL.

**Keywords** Local brittle layer · Electro-gas weld metals · EG70T-G wire

## 1 Introduction

During the past several decades, the relationship between the microstructure and mechanical properties of high-strength steel welds having a tensile strength over 500 MPa has been extensively studied with an effort to improve the strength and toughness of steel welds by controlling the weld microstructures [1–4]. Recently, similar efforts have been made for the welds deposited by high heat input welding processes like electro-gas welding as it becomes popular in the shipbuilding industries and others to enhance welding productivity [5–9]. Following these efforts, it is presently well accepted that weld

microstructures primarily consisting of acicular ferrite provided optimum mechanical properties especially from the perspective of toughness attributing to its fine nature in grain size. On the other hand, the formation of other major constituents such as grain boundary ferrite and ferrite with a second phase led to the deterioration of weld toughness, as their grain sizes were normally much coarser than that of acicular ferrite. Thus, common approaches have been made in a way to maximize the acicular ferrite content with a concurrent decrease in other constituents not only for single pass [10, 11] but also for multi-pass steel welds [12–14].

However, in the case of the multi-pass weldment, the situation becomes much more complicated due to the increased heterogeneity within the weld microstructure resulted from the addition of a range of reheated microstructures. These are different from the as-deposited microstructures to a varied extent depending on the peak temperatures of weld thermal cycles given by the subsequent passes and their cooling rates [15]. This, in turn, can render local changes in mechanical properties and especially in the impact toughness of the weld metals [16–19]. Accordingly, for a better understanding of the relationship between microstructure and mechanical properties, researchers often prefer to employ the as-deposited weld metals made via one-pass welding techniques [10, 20, 21]. In these studies, it should be pointed out that all the mechanical

---

Recommended for publication by Commission IX - Behaviour of Metals Subjected to Welding

---

✉ Hee Jin Kim  
kimheejin0827@gmail.com

<sup>1</sup> Division of Materials Science and Engineering, Hanyang University, 222 Wangsimni-ro, Seongdong-gu, Seoul 04763, Republic of Korea

<sup>2</sup> Korea Institute of Industrial Technology (KITECH), 156 Gaetbeol-ro, Yeonsu-Gu, Incheon 21999, Republic of Korea

<sup>3</sup> R&D Center, KISWEL, 704 Gongdan-ro, Seongsan-gu, Changwon-si, Gyeongnam 51544, Republic of Korea

test specimens were extracted mostly from a single location, that is, the central region of a welded joint, without any concern toward possible variations of weld properties within a single-pass weld deposit. It follows that in the case of Charpy V-notch (CVN) impact specimens, the notches for weld deposits are generally machined at the weld centerline transverse to the welding direction and then, the values obtained are regarded as representing the overall weld toughness. In contrast, HAZ specimens are normally forced to be prepared at several locations at or near the fusion line since the HAZ toughness has been well established to vary greatly with the distance from the fusion line.

Somewhat like HAZ, the single-pass weld metals deposited via electro-gas or electro-slag welding processes appeared to exhibit a toughness variation yielding the lowest values at the weld centerline [22–26]. As is well described in reference [5, 22], these two processes are basically done in the vertical up position and capable of making a single-pass weld for any plate thickness with a relatively high level of heat input. In shipbuilding industries, electro-gas welding is widely used for vertical position welding of sheer strakes and hatch side coamings of large container ships and with a tandem version using two electrodes [6], and is currently capable of welding thick plates up to 80 mm by a single pass. By the way, in a report investigating a variety of electro-slag welded joints [24], the varied impact toughness results with a minimum at the weld center were well illustrated by using two-dimensional contour lines drawn on the transverse cross-sections, although the data points were quite limited. One of his results obtained for a 76-mm-thick A36 plate showed a CVN toughness of 22 J at the weld center compared to 72 J recorded in the surrounding area.

Referring to the above studies, it seems to be quite evident that weld toughness is no longer uniform even within a single-pass weld, at least when the welds become large scaled, suspecting that the microstructure at weld centerline might be different from that of the adjacent areas to result in a toughness drop at the weld center. However, to the best of our knowledge, there has been scarce information in the welding literature regarding the metallurgical factors that can cause toughness drop at the weld center until our previous study reporting the microstructural characteristics of a tandem electro-gas weld metal from the local brittleness point of view [27]. What we have observed was the formation of a thin layer of brittle microstructure at the weld centerline with a width of about 2 mm, and this layer has been referred to as “local brittle layer (LBL).” In this report, the local brittleness at LBL was determined to be attributable to the formation of longitudinally grown columnar grains whose boundaries were fully decorated with longitudinal veins of coarse grain boundary ferrite grains, making cracks easy to propagate through these

veins aligned in the crack propagation direction. These observations seemed to be sufficient to explain why local brittleness only occurred at the weld center of the electro-gas weld studied but there were still several points that required clarification or characterization. These points are the subject of the present investigation.

1. As mentioned above, in C-Mn or HSLA steel welds, weld metal toughness is greatly affected by the weld microstructure. Therefore, weld microstructure is often quantified in terms of the proportion of three major microstructural constituents: grain boundary ferrite, ferrite with the second phase, and acicular ferrite. As these three constituents differ greatly in grain size, weld toughness tends to decrease with an increased fraction of coarse constituents such as grain boundary ferrite or ferrite with the second phase. Therefore, in addition to the directional factor of columnar grains, the possible variation in the proportion of grain boundary ferrite and ferrite with the second phase across the weld centerline should have been studied as well. In the present study, therefore, it was attempted to quantify the weld microstructures revealed at the same locations as CVN notches were made in the previous study [27]; the obtained results were then correlated with the toughness profile given in the previous report.
2. In the previous report [27], the formation of LBL was realized from the results of the toughness profile measured from the centerline (LBL region) to the side of the weld (non-LBL region). For the sake of comparison, Charpy specimens taken from different locations were tested at a single temperature of 0 °C, which was selected without any background. This meant that if the specimens were tested at other temperatures, the extent of toughness drop at LBL would be far different from that reported. Considering the ductile-brittle transition behavior of the impact properties, toughness variation could not take place across the weld if the test temperature was so low as to make all regions of weld metal brittle. Therefore, it was of our subsequent interest to define the LBL brittleness in terms of the CVN ductile-brittle transition temperature instead of the CVN impact toughness value at a given temperature and then to compare the results with those obtained from the surrounding non-LBL region. In this context, this study attempted to construct the CVN transition curves for two different locations to quantify the LBL brittleness in terms of the transition temperature.
3. Another factor that could affect weld toughness was the content of the microphases, which may act as a crack initiation site. Many researchers [28–30] have found cleavage cracks to initiate at non-metallic inclusions formed in welds. However, the previous study did not give any attention to the possible variation in inclusion content across the weld centerline.

## 2 Experimental procedure

### 2.1 Materials used

Three EG welded joints were employed in this investigation: two two-pole (tandem) EG welds were made with steel plates of different thickness, 80 and 73 mm, and one one-pole EG weld was fabricated with a 25-mm-thick plate, each weld being indicated as tandem EG(80t), tandem EG(73t), and one-pole EG(25t), respectively. The tandem EG(80t) weld was the one that has been used for the previous investigation [27] and the others were newly fabricated for the present study using different wires and base plates in order to change the weld microstructure, especially in a way to lower the content of grain boundary ferrite. The base plates used for each weld are listed in Table 1. BM(1) and BM(2) are 500-MPa class low-carbon high-tensile steels classified as AH36 and EH36 in IACS UR W-11 [32], and BM(3) is a high-carbon A516-70 grade steel [33]. The total length and width of the welded plates were 500 and 300 mm, respectively. As the heat input of electro-gas welding decreases with decreasing the plate thickness, the thinner the base plate, the faster the cooling rate. For the one-pole electro-gas welding process, Kojima and others [31] have performed a numerical analysis on the weld thermal cycles providing a chart of master curves which presents the cooling time from 800 to 500 °C at the fusion line for the plate thickness up to 55 mm and for the heat input up to 50 kJ/mm. Extrapolating the curves up to the present welding conditions, the cooling times from 800 to 500 °C,  $\Delta t(8/5)$  in Table 1, could be estimated to be 500, 400, and 220 s for tandem EG(80t), tandem EG(73t), and one-pole EG(25t), respectively. Accordingly, with increasing the cooling rate by using thinner steel plates, the weld microstructures at the same or higher alloying content could be changed to contain a less amount of grain boundary ferrite, which enables to investigate the LBL formation as a function of grain boundary ferrite content. All welds were fabricated using 1.6-mm flux-cored wires slightly different in chemistry but safely classified as EG70T-G in AWS A5.26/A5.26M-97 [34]. For example, the wire used for tandem EG(73t) was the one designed to have high contents of nickel and manganese. Pure CO<sub>2</sub> gas was used for shielding.

The welding conditions and the groove designs for these welds are presented in Table 1. As expected, there was a large difference in heat input due to the differences in the thickness and groove area. Figure 1 shows macro views of the bulk specimens that were etched to display the macrostructures on their top transverse sections, which were perpendicular to the welding direction (WD). The chemical composition of the welds was determined at the central region of the mid-thickness using a OBLF Model QSN750-II spark emission spectrometer except for oxygen that was determined by the inert fusion method using a Leco Model ON836 analyzer. The results are listed in Table 2 along with those of the base plates. Note that the weld metals are similar in oxygen content but somewhat different with regard to C, Mn, Ni, and B content, all of which are hardening elements.

### 2.2 Mechanical tests

A number of standard CVN impact specimens were extracted from the middle part of the welds with their notches parallel to the weld centerline. Figure 2 shows the macrostructure of tandem EG(80t) weld illustrating the location of CVN specimens, their notches being right at the weld centerline (coded as “CL+0”) or apart from the weld centerline by  $x$  mm (coded as “CL+ $x$ ”). For tandem EG(73t) weld, CVN specimens were taken at five different locations and tested at a fixed temperature of  $-20$  °C to confirm the formation of LBL in this weld. In the case of the other two welds, a sufficient number of specimens were prepared at two locations: CL+0 and CL+6 for EG(80t), and CL+0 and CL+5 for EG(25t). These were tested at various temperatures to establish the full ductile-brittle transition curves for the two locations. After the test, some of the EG(80t) specimens were subjected to fractographic analysis using a scanning electron microscope (SEM) to see the change in fracture mode relating to the microstructural characteristics of LBL. Besides, some brittle specimens of EG(73t) were sectioned to examine relating to the underneath microstructure along the crack path.

Standard tensile specimens were also machined from the central portion of each weld metal and the results are listed in Table 3 along with the hardness values. The tensile strength of

**Table 1** Welding conditions and groove geometries used for the three EG welds studied in this investigation

Weld ID	Groove geometry		Welding conditions				$\Delta t(8/5)^* \text{ s}$
	Groove angle	Root gap	Current	Voltage	Speed	Heat input	
Tandem EG(80t)	16°	12 mm	400 A/380 A	40 V/38 V	25 mm/min	73 kJ/mm	500
Tandem EG(73t)	20°	10 mm	360 A/350 A	36 V/35 V	32 mm/min	47 kJ/mm	400
One-pole EG(25t)	20°	10 mm	360 A	35 V	39 mm/min	20 kJ/mm	220

$\Delta t(8/5)^*$ : cooling time from 800 to 500 °C estimated using a chart given in reference [31]

**Table 2** Chemical composition of the EG weld metals (WM) and base metals (BM) in wt.%

Weld ID		C	Si	Mn	P	S	Ni	Al	Ti	B	O
Tandem EG(80t)	WM	0.06	0.25	1.44	0.008	0.002	1.07	0.010	0.025	0.0028	0.0349
	BM(1)	0.08	0.31	1.55	0.008	0.001	0.01	0.030	0.010	0.0004	-
Tandem EG(73t)	WM	0.05	0.19	1.66	0.009	0.009	1.49	0.008	0.032	0.0043	0.0383
	BM(2)	0.06	0.17	1.57	0.005	0.001	0.21	0.033	0.016	0.0008	-
One-pole EG(25t)	WM	0.09	0.16	1.33	0.010	0.005	1.17	0.011	0.035	0.0039	0.0394
	BM(3)	0.20	0.36	1.07	0.012	0.000	0.01	0.026	0.001	0.0001	-

BM(1): AH36, BM(2): EH36, BM(3): A516-70

present electro-gas welds was noted to be well over 480 MPa, the minimum strength required for EG70T-G.

### 2.3 Weld microstructure

In general, weld microstructures are examined on the surfaces of transverse sections like the one designated as “T-plane” in Fig. 3. However, in electro-gas welds, the transverse macrostructure alone was found to be insufficient to obtain full details with regard to weld solidification structures due to their 3-dimensional variance across the weld centerline [27]. Considering this, the macro specimens of EG(80t) weld were further sectioned along the longitudinal directions to investigate the weld microstructures on two different planes: one through the mid-thickness (designated as the “L-plane”) and the other parallel to the weld centerline (designated as the “LT-plane”). In the case of the LT-plane, the one taken apart from the weld centerline (CL) by a distance of  $x$  mm was referred to as “LT(CL+ $x$ ).” It was worth noting that LT(CL+ $x$ ) plane was identical to the fracture plane of the CVN impact specimen notched at CL+ $x$ . For tandem EG(80t) weld, a number of optical microscope (OM) specimens were taken at the locations identical to CVN notches and then, microstructural analyses were performed on their LT(CL+ $x$ ) planes. Firstly, the specimens were etched with a 2% Nital solution and observed via OM. From the OM images, the proportion of

microstructural constituents was measured by the point-counting method. The same surfaces were also used in un-etched conditions for analyzing non-metallic inclusions in terms of their size and number density. For each specimen, a total of 20 OM pictures were obtained at  $\times 500$  magnification, covering an area of about  $0.86 \text{ mm}^2$ . Under this condition, inclusions larger than  $0.4 \text{ }\mu\text{m}$  could be taken into account.

## 3 Results and discussion

### 3.1 Microstructural characteristics of the LBL in tandem EG(80t) welds

As pointed out previously [27], the columnar structure of a tandem EG(80t) weld metal will look very different depending on where the specimen is taken and which plane is etched for examination. To illustrate the difference in detail, OM specimens extracted from two different locations (CL+0 and CL+6, marked with square dots in Fig. 3) were examined via three different planes, i.e., T-, L-, and LT-planes. Figures 4 a and b show the three micrographs and combined to visualize the three-dimensional morphology of columnar grains, their boundaries being delineated by veins of grain boundary ferrite. At the location of CL+0 (Fig. 4a), a bundle of straight columnar grains growing in the welding direction (normally

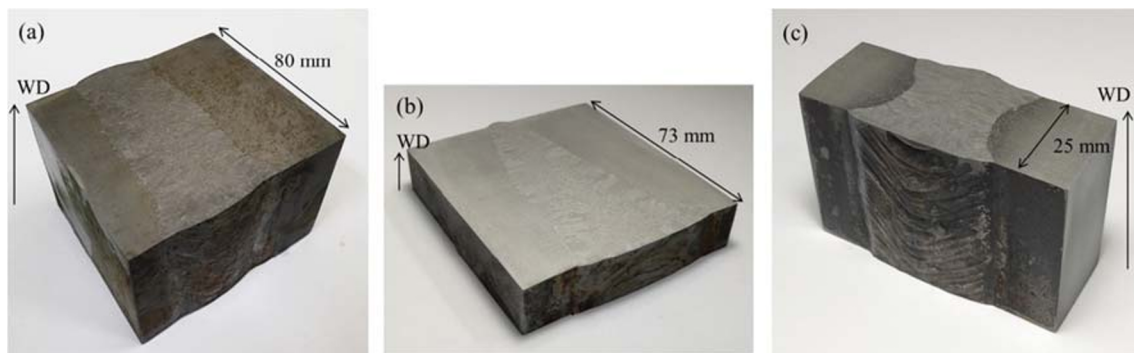


**Fig. 1** Macro views of EG weld blocks revealing transverse macrostructures: **a** tandem EG(80t), **b** tandem EG(73t), and **c** one-pole EG(25t) weld. Arrows indicate the welding direction (WD)

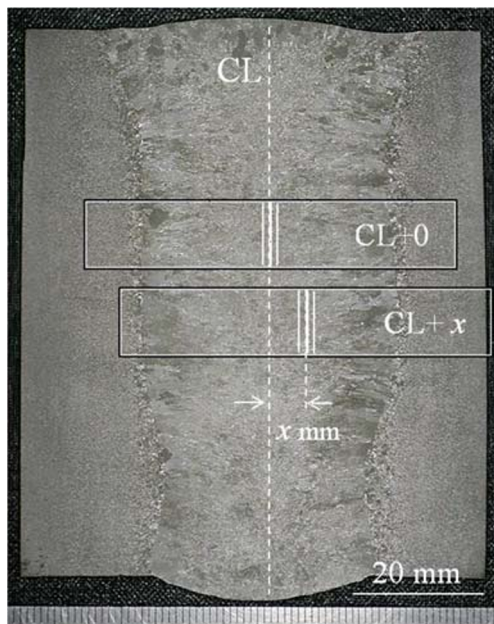


**Fig. 2** Transverse macrostructure of a tandem EG(80t) weld and a schematic representation of the impact specimens prepared with their notches at weld CL(CL+0) and  $x$  mm apart from CL(CL+x)

referred to as the longitudinal direction) were observed and these grains turned out to be equiaxed on the T-plane. On the other hand, at the location of CL+6 (Fig. 4b), the columnar grains initially developed from the fusion line and grew in the transverse direction with successive changes toward the upward direction as they approached to the weld centerline. As a result, the shape of the columnar grains at CL+6 appeared to be equiaxed on the LT-plane and elliptical on the T-plane. Comparing the L-plane microstructures of two locations, it can be seen that EG(80t) weld possessed two groups of columnar grains distinctly different in growth direction: one group standing in the purely vertical direction and the other group lying transversely but inclined upwards as it approached to the centerline. This indicates that during solidification, these two columnar structures will meet somewhere in the L-section resulting in a sort of transition in growth direction from inclined to purely vertical. Indeed, this transition was confirmed to take place in this weld at around CL+1 as shown in Fig. 5. This type of transition in columnar structure has been reported by Komizo and others [35] to occur in the electron-beam weld metal made at a low travel speed and

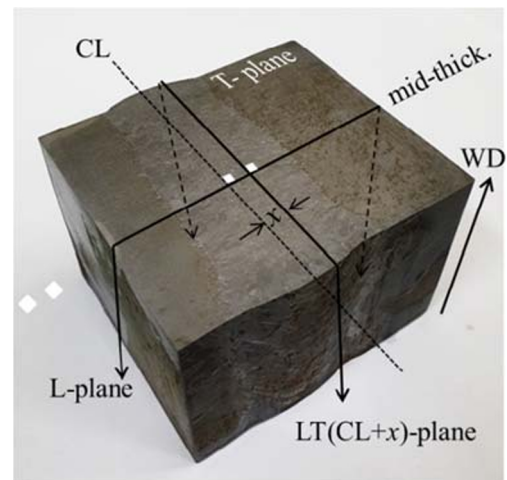


**Fig. 3** Transverse macro section specimen of a tandem EG(80t) weld revealing microstructures on the longitudinal L- and LT-planes

was designated as a “raft structure” which was one out of four different types, that being raft, elongated, equiaxed, and interlocking in order of increasing travel speed. As the travel speed of the electro-gas welding process is basically very low, it is most likely that the raft type would be the one that can be formed in the electro-gas welds.

Another thing to note in Figs. 4 and 5 is that the EG(80t) weld microstructure consists primarily of grain boundary ferrite outlining the columnar grain boundaries and intragranular ferrite enclosed by grain boundary ferrite veins with a minimal fraction of ferrite with the second phase. The grain boundary ferrite grains were coarse as to an average size of  $50\ \mu\text{m}$  and some were very long with a maximum length of  $\sim 600\ \mu\text{m}$ . On the other hand, the intragranular ferrite grains were more or less similar to acicular ferrite but mixed with a rather coarse ferrite having an irregular shape. The size of the intragranular grains was so fine that they were measured via SEM at 1000 magnification and turned out to be  $3.7\ \mu\text{m}$  on average with the largest size being  $10.1\ \mu\text{m}$ .

Of the microstructures taken from three planes, the LT-plane microstructure would be the most relevant to weld toughness because CVN fractures propagate parallel to this plane and thus was in terms of the proportion of grain boundary ferrite. Figure 6 shows the result plotted as a function of the distance from the weld centerline (CL+0) and this result was overlapped with the CVN test results from the previous

**Table 3** Tensile properties and hardness of weld metals investigated

Weld ID	Tensile properties			Hardness Hv10
	Yield strength MPa	Tensile strength MPa	Elongation %	
Tandem EG(80t)	434	550	28	183
Tandem EG(73t)	445	592	28	202
One-pole EG(25t)	476	617	23	206

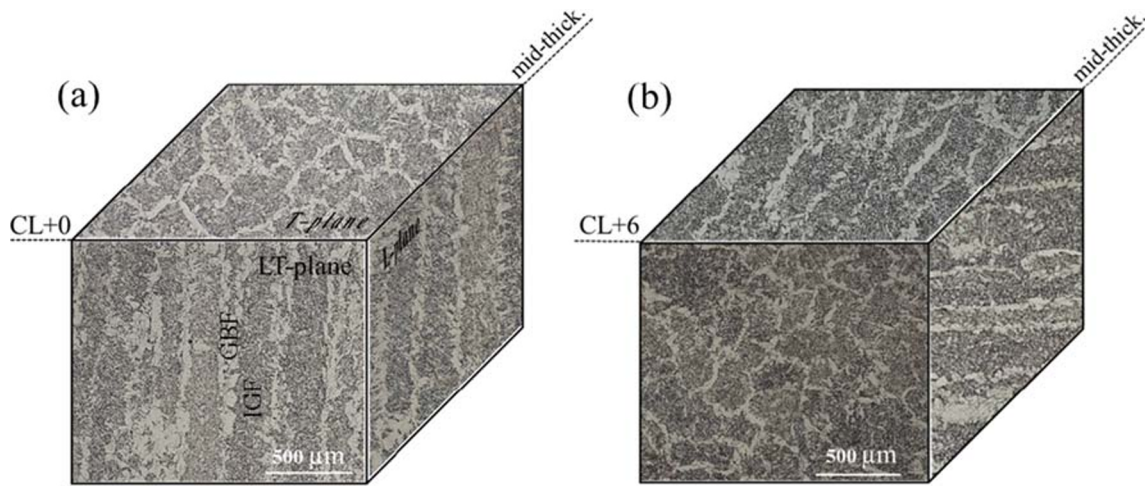


**Fig. 4** Three-dimensional (3-D) microstructures of tandem EG(80t) weld constructed for the two different locations marked by white dots in Fig. 3: **a** CL+0 and **b** CL+6

report [27]. First, it is evident that a large variation in grain boundary ferrite content takes place near the weld center with a maximum value being recorded to be 48% at the centerline. This result indicates that the weld microstructure of EG(80t) weld is no longer uniform, especially in the content of grain boundary ferrite, and that this is most likely due to the transition of columnar structures near the weld centerline as described above. Secondly, correlating the toughness results, one could notice at a glance that there exists a well-known negative influence of grain boundary ferrite on impact toughness; the higher the grain boundary ferrite content, the lower the impact toughness. Looking closely, however, it is of interest to notice the very little difference in grain boundary ferrite content between CL+1 and CL+3 even while a big difference in CVN impact toughness presents between these two locations. In order to illustrate such an unusual relation, the two curves in Fig. 6 were reconstructed to show the CVN impact energy as a function of grain boundary ferrite content as

shown in Fig. 7. In this figure, there were two groups of data points far different in impact toughness: the upper line was constructed with three data points for CL+3, CL+6, and CL+8 and the lower line with the other three locations encompassed in LBL of the present EG(80t) weld. This result well illustrates a great difference in CVN impact toughness between CL+1 and CL+3 even at the same level of grain boundary ferrite content (ca. 35%). Because of this, this difference in impact toughness needed to account for some other factors, the most responsible one being considered to be the morphological difference in grain boundary ferrite veins shown in Fig. 8.

Figure 8 shows the OM microstructures taken from two LT-planes at CL+1 and CL+3. At CL+1, most of the columnar grains aligned in the longitudinal direction similar to those in CL+0 and produced long and straight veins of grain boundary ferrite running parallel to crack propagation direction. The occurrence of preferential crack propagation through the grain boundary ferrite veins could be suspected with the vertical streak patterns revealed on the fracture surface as shown in Fig. 9a and with the fractographic features observed via SEM as will be described later. In contrast, the grain boundary

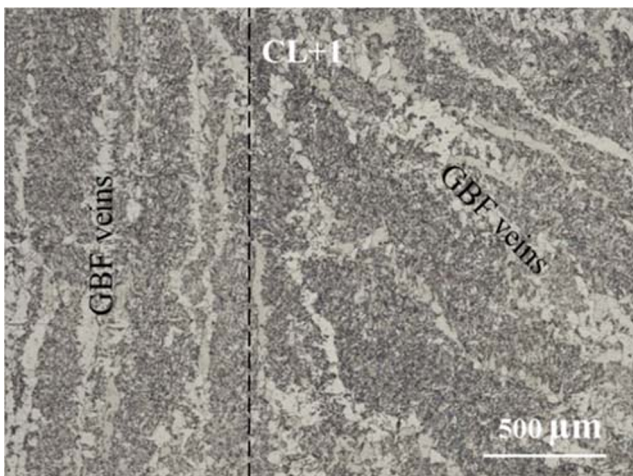


**Fig. 5** OM micrograph taken from the L-plane showing the growth direction transition of columnar grains at CL+1. Note the columnar grain boundaries are delineated by veins of grain boundary ferrite (GBF)

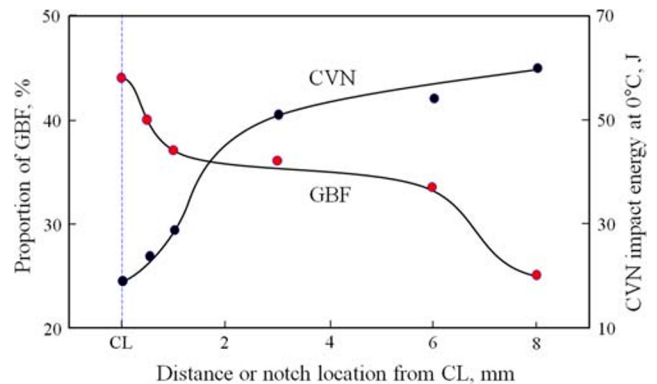


**Fig. 6** The result of microstructural analysis illustrating the proportion of GBF varying with the distance from CL. CVN results quoted from reference 27 are included

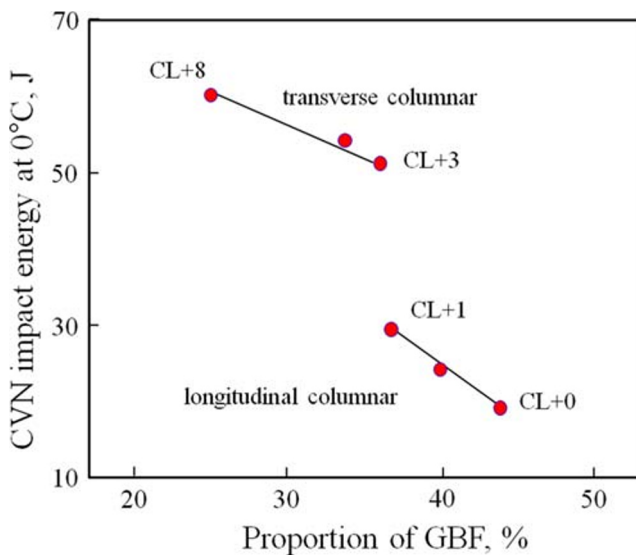


**Fig. 7** CVN impact toughness plotted as a function of grain boundary ferrite (GBF) content in tandem EG(80t) weld

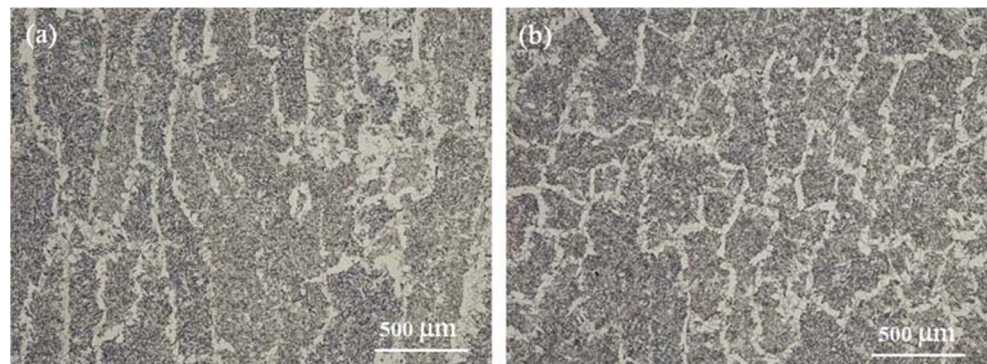
ferrite veins at CL+3 had a sort of network structure as shown in Fig. 8b. With this type of network morphology, a crack will propagate cutting through these veins so that streak patterns cannot be developed on the fracture surface as shown in Fig. 9b. It followed with the conclusion that the toughness drop pronounced between CL+1 and CL+3 in Fig. 7 is mainly due to the morphological change in ferrite veins from network type to parallel type on the fracture plane and this factor would be the most critical for the formation of LBL in the electro-gas weld metals when the grain boundary ferrite forms to a large extent enough to provide the preferential crack path.

As mentioned earlier in the introduction, the presence of LBL in tandem EG(80t) welds has been verified by the occurrence of a sudden drop in impact toughness when approaching to the weld centerline as shown in Fig. 6. Figure 7 shows the extent of this drop is greater than 20 J. As C-Mn steel welds undergo ductile-brittle transition with decreasing the temperature, however, the extent of toughness drop would be varied depending on the test temperature as mentioned earlier. In order to overcome the temperature dependence, it was proposed to construct the ductile-brittle transition curves and to

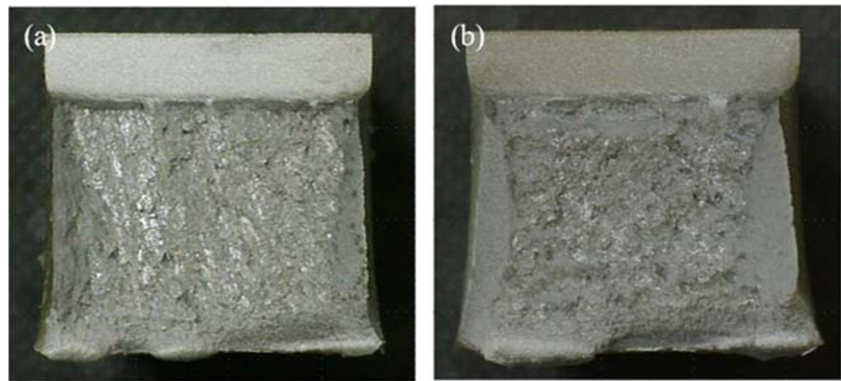
assess the relative brittleness of LBL in terms of the difference in transition temperature between LBL and non-LBL regions. This study selected CL+0 and CL+6 representing LBL and non-LBL regions, respectively. The full transition curves constructed for the two locations can be seen in Fig. 10. From these two curves, the transition temperature, determined at 100 J that is roughly one-half of the upper-shelf energy, is about 20 °C for CL+6 and somewhere from 60 to 80 °C for CL+0, implying that the difference in transition temperatures is as much as 50 °C. This result also indicates that the toughness drop at LBL would be about 120 J if the CVN tests were performed at 40 °C instead of 0 °C. Another fact that could be noted in Fig. 10 was that the curve for CL+0 exhibited a stepwise transition accompanying the introduction of an intermediate shelf at around 100 J. To ensure the intermediate shelf being present, three specimens were tested at the temperatures lying in the intermediate range while a single specimen at other temperatures. The intermediate shelf extending from 50 to 80 °C had CVN toughness of about 100 J. Such a stepwise transition seemed to be very unusual and has not been reported in the open literature.

A mechanism for the stepwise transition is discussed from the perspective of LBL microstructural characteristics. As shown in Fig. 4a, the LBL microstructure in the LT-plane consisted of a layered structure constructed with coarse grain boundary ferrite stripes alternating with fine intragranular ferrite ones. When these two microstructures are greatly different in grain size, their inherent transition temperatures would be far different so two transition curves far apart could be drawn as the schematic curves in Fig. 11: “IGF” and “GBF” are representing intragranular ferrite and grain boundary ferrite respectively. If these two microstructures were packed layer by layer like LBL microstructure, the resultant composite would have possessed a transition curve constructed by averaging the two curves as presented by the “IGF + GBF” curve in Fig. 11. Due to a large difference in transition temperature between GBF and IGF, the “IGF + GBF” curve comes to have a step in its transition curve that can be called an “intermediate shelf.” At the intermediate shelf temperature, the GBF layer is brittle while IGF is ductile. This feature was clearly verified

**Fig. 8** OM microstructures taken from LT-planes of tandem EG(80t) weld at **a** CL+1 and **b** CL+3



**Fig. 9** Fracture appearance of broken Charpy specimens of tandem EG(80t) weld representing **a** CL+1 and **b** CL+3



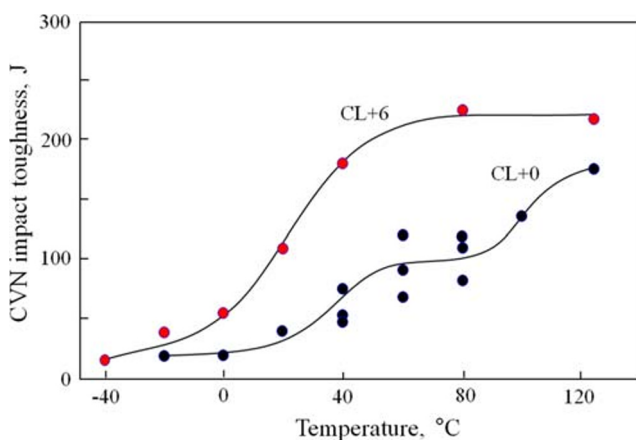
via the SEM examination of broken Charpy specimens and one example is given in Fig. 12. Vertical streak patterns are well noted in the macro view of the fracture surface shown in Fig. 12a. Figure 12b showing the SEM fractograph taken from the region near the notch front clearly demonstrates the layered appearance of alternating ductile microvoid coalescence and brittle cleavage modes. This result well verifies the hypothesis made in Fig. 11.

Figure 12b also shows a cleavage facet that was appeared to be initiated from the non-metallic inclusion marked by an arrow and its detail is further presented in Fig. 12c. This result confirms the fact that inclusions can act as crack initiation sites of cleavage facets. From this finding, it was of additional concern that LBL toughness could be affected by inclusions if the inclusion content were high in the LBL region. Table 4 shows the results of the inclusion analysis performed on the LT-planes of interest. As is evident from this table, there is little change in inclusion size but an appreciable variation in inclusion density, indicating that electro-gas welds would not be uniform in inclusion characteristics, at least in inclusion density. The inclusion density being the highest at CL+0 may imply that the LBL brittleness is partly attributable to the high inclusion density at the LBL. However, the adverse

effects of the increased density could not be accessed in detail and were remained for further investigation in the future. One thing to note in this table, however, is that there is no sharp change in inclusion density at CL+1 unlike the microstructural transition shown in Fig. 5, indicating that the variation in inclusion density would be far less critical than the factors relating to grain boundary ferrite.

### 3.2 Effect of grain boundary ferrite content

Referring to the results of tandem EG(80t) welds described above, it became clear that the low toughness at LBL was attributable to the formation of parallel veins of grain boundary ferrite, and thus, it could be suspected that the extent of toughness drop at LBL could be minimized by suppressing the grain boundary ferrite being formed during cooling. To confirm this hypothesis, tandem EG(73t) weld was made with increased Ni and B content (Table 2) to enhance the hardenability and with the increased cooling rate by lowering the heat input. Figure 13a shows the low-magnification OM microstructure taken from the LT-plane at CL+0 which clearly displays parallel veins of grain boundary as have seen for tandem EG(80t) weld in LT-plane of Fig. 4a. Compared to



**Fig. 10** CVN ductile-brittle transition curves of tandem EG(80t) welds for CL+0 and CL+6. Note: the CL+0 represents LBL and CL+6 represents the non-LBL region

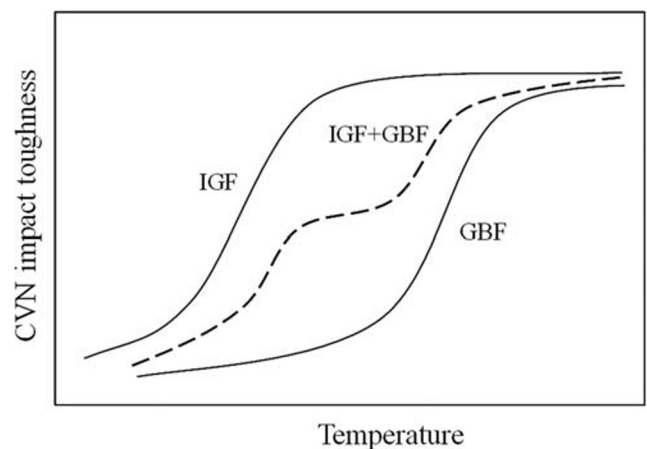


**Fig. 11** Schematic illustration of the mechanism for the stepwise transition that occurred in the LBL composed of grain boundary ferrite (GBF) and intragranular ferrite (IGF)



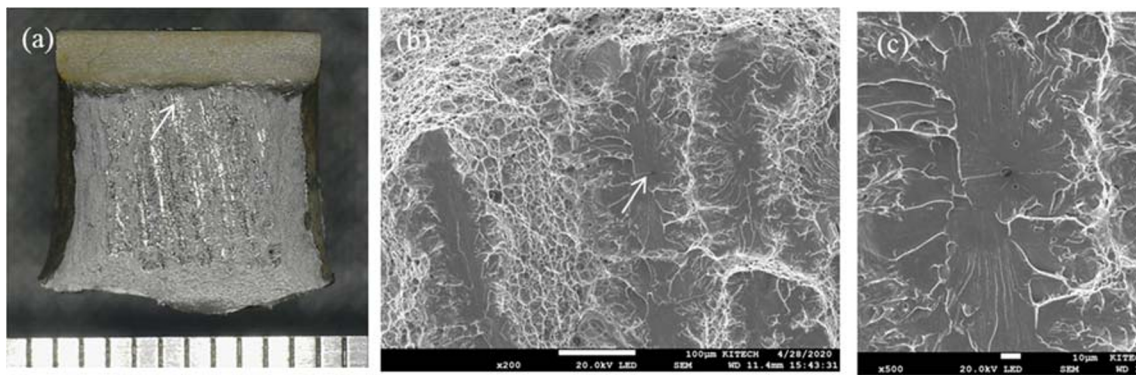


**Fig. 12** Fracture surface of Charpy specimens tested at 60 °C: **a** macro view of the fracture surface, **b** SEM fractograph taken from the region marked by an arrow in **a** and **c** high-magnification SEM picture taken at the inclusion marked by an arrow in **b**

tandem EG(80t) welds, however, the present EG(73t) weld has much thinner veins and the grain boundary ferrite content at CL+0 was measured to be 19%, which was much less than that of EG(80t) weld, 44%. Considering the decreased content of grain boundary ferrite, CVN impact tests for EG(73t) weld were performed in a way to see the toughness variation across the weld centerline and thus to identify LBL formation in this weld; the results are presented in Fig. 14. This result demonstrates that this weld still formed LBL at its weld center but compared to EG(80t) weld, the LBL toughness improved significantly from 19 to 40 J with decreasing grain boundary ferrite content.

After sectioning the fracture surface of the CL+0 specimen, the cross-section was examined in OM and the results are displayed in Fig. 13b and c. As expected, CVN crack was observed to propagate mainly through the ferrite veins as shown in Fig. 13b. In this OM micrograph, a few grain boundary ferrite grains locating underneath the fracture surface were found to be cracked during the fracture process as shown more clearly in the enlarged OM micrograph of Fig. 13c. This feature was also observed in the EG(80t) weld [27]. These and previous results indicate that the grain boundary ferrite grains are so large and brittle that they tend to be prematurely fractured promoting crack to propagate through these veins.

**Table 4** Result of inclusion analysis performed on the LT-plane of EG(80t) weld

Location	No. of inclusions counted	Density (/mm <sup>2</sup> )	Size (μm)
CL+0	1599	1868	1.09
CL+1	1521	1777	1.08
CL+3	1318	1540	1.13
CL+5	1210	1413	1.18
CL+6	1203	1405	1.20
CL+8	1240	1448	1.16

To suppress the LBL formation further by minimizing the grain boundary ferrite formation, an additional EG weld was fabricated with a lower heat input of one-pole EG welding using a 25-mm-thick high-carbon A516-70 steel plates. A macro view of this weld is presented in Fig. 1c and its chemical composition in Table 1. First of all, the centerline microstructure at LT(CL+0) plane was observed to see if grain boundary ferrite veins formed or not. As shown in the OM micrograph of Fig. 15, this weld was nearly absent from grain boundary ferrite and thus, no ferrite veins were observed. Due to the absence of ferrite veins, the grain boundaries of columnar grains were difficult to trace and the arrows in this micrograph indicate a part of the boundary that was distinguishable via high-magnification OM examination. Accordingly, it was assumed that there would be little change in CVN toughness across the weld centerline and thus, no LBL would be produced. Under this assumption, the impact tests for this weld were planned to construct the full ductile-brittle transition curves for two different locations: CL+0 and CL+5. As shown in Fig. 16, two curves are very close to each other and thus, their transition temperatures are nearly identical given the slight difference in upper-shelf energy. Hence, it could be concluded that no LBL formed in this EG(25t) weld due to little formation of grain boundary ferrite. Another thing to note in Fig. 16 is that their transition temperatures lowered substantially down to −60 °C and thus, the CVN impact toughness at low temperature improved significantly compared to tandem EG(80t) and EG(73t) welds. This and previous results imply that the amount of grain boundary ferrite formed at the weld centerline is the most critical factor that determines not only the LBL formation but also the level of CVN toughness at the weld center of EG welds. This can be drawn only when the weld microstructure is predominant with fine acicular ferrite without forming ferrite with a second phase or bainite. Considering the strong dependence of LBL formation on the content of

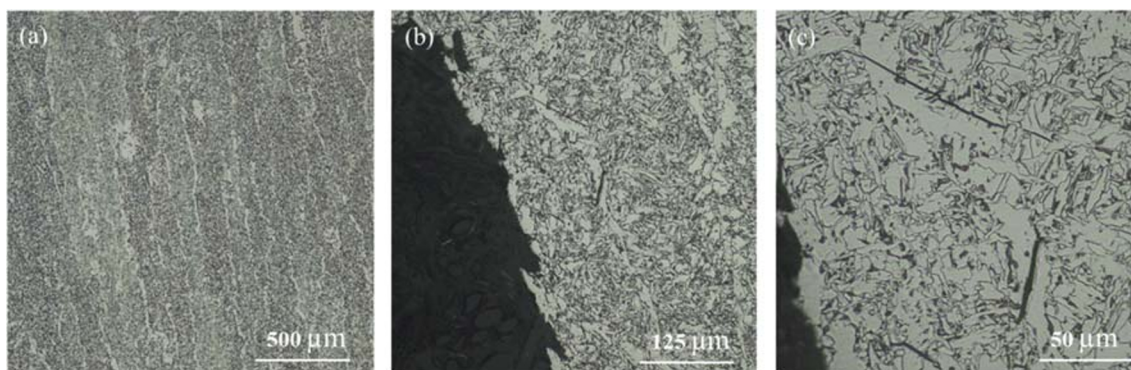


**Fig. 13** OM microstructures of tandem EG(73t) weld taken from **a** the LT(CL+0) plane, **b** the cross-section of fracture plane showing the preferential crack propagation along the veins of grain boundary ferrite, and **c**

grain boundary ferrite grains cracked in the region slightly below the main fracture surface

grain boundary ferrite formed, it could be suggested that LBL-free electro-gas welds will be obtained either by controlling the cooling rate and/or by adjusting the weld chemistry to cope with given heat input. Previously, it was shown that, for 51-mm-thick plate EG welded with 30 kJ/mm, grain boundary ferrite turned out to be nearly absent when the carbon equivalent with  $C_{eq}(WES)$  equation increased over 0.37 [6]. In the case of electro-slag welding, a similar weld was also reported to be obtained by controlling the boron/nitrogen ratio [11]. These results suggest that the LBL formation could be eliminated by selecting welding wires with a sufficient hardenability at a level of heat input being employed. Accordingly, it could be suggested for the welding wires of electro-gas welding, as the heat input of electro-gas welding process is largely determined by the thickness of the plates being welded, to provide the users with additional information on the heat input range recommended or the CVN toughness expected at different levels of heat input.

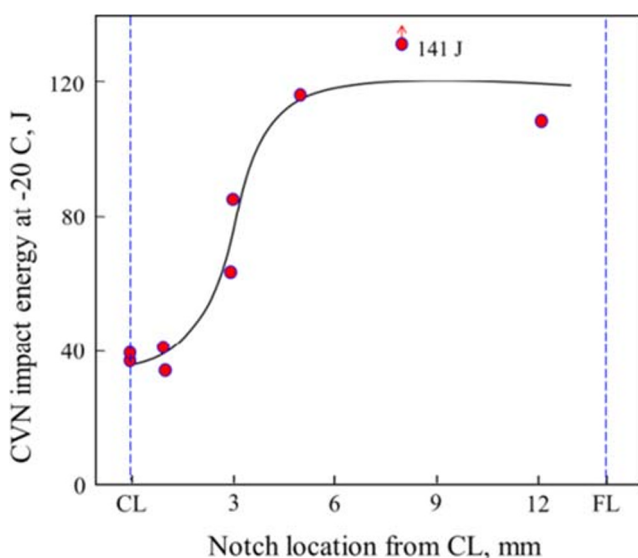


**Fig. 14** Variation of impact toughness with distance from the weld centerline (CL) in tandem EG(73t) weld

## 4 Conclusion

1. The LBL microstructure formed at the centerline of EG weld metal consists of two products transformed from the longitudinally grown columnar grains: grain boundary ferrite veins formed at columnar grain boundaries and intragranular ferrite formed within the grains and outlined by veins. As grain boundary ferrite veins run parallel to crack propagation direction, the proportion of grain boundary ferrite formed is found to be the most critical factor that determines LBL formation and controls the CVN toughness of LBL. Thus, the detrimental effects of grain boundary ferrite on LBL toughness could be alleviated by decreasing the content of grain boundary ferrite and eventually eliminated by making weld microstructure free from grain boundary ferrite through the proper selection of welding wires with a sufficient hardenability at a level of heat input being employed.
2. The LBL brittleness could be accessed by constructing the CVN ductile-brittle transition curve for the weld

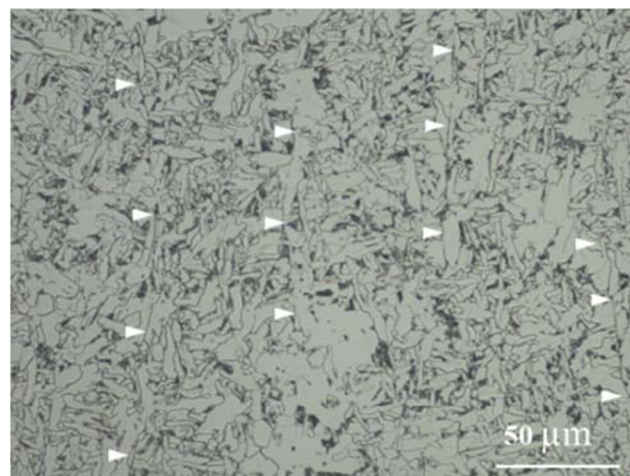


**Fig. 15** OM microstructure of one-pole EG(25t) weld taken at the weld centerline of the L-plane. Arrows indicate the trace of columnar grain boundaries

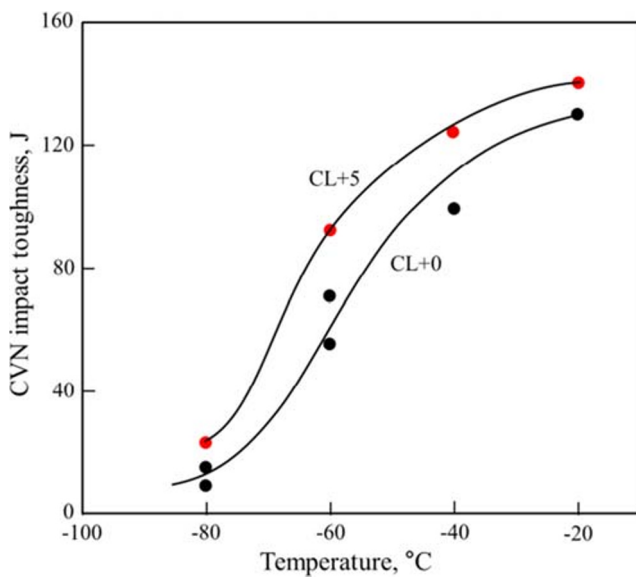


**Fig. 16** Ductile-brittle transition curves of one-pole EG(25t) weld for CL+0 and CL+5

centerline and then comparing it with that of the non-LBL region. Its extent could be quantified in terms of the difference in transition temperatures measured from these two curves. With grain boundary ferrite formed to a large extent, the transition curve for LBL would show a step-wise transition with the introduction of an intermediate shelf most likely due to the layered structure alternating veins of coarse grain boundary ferrite with stripes of fine intragranular ferrite.

- EG welds showed a variation in inclusion density with its maximum at the centerline and thus, LBL brittleness could be suspected to be partly attributable to its high inclusion density. However, its effect appeared to be minimal compared to the role of grain boundary ferrite but needs further investigation.

## References

- Ohkita S, Horri Y (1995) Recent development in controlling the microstructure and properties of low alloy steel weld metals. *ISIJ Int* 35(10):1170–1182
- Grong O, Matlock DK (1986) Microstructural development in mild and low-alloy steel weld metals. *Int Metal Rev* 31(1):27–48
- Farrar RA, Harrison PL (1987) Acicular ferrite in carbon-manganese weld metals: overview. *J Mater Sci* 22:3812–3820
- Levine E, Hill C (1977) Structure-property relationship in low C weld metal. *Met Trans A* 8A(9):1453–1463
- Takeuchi N, Nagashima M, Tsuruga S (1985) Automated welding in tank construction and its cost-reducing effect. *Weld J* 84(2):18–29
- Hashiba Y, Kojima K, Kasuya T, Kumagai T (2015) Development of welding consumables and welding process for newly developed steel plates. *Nippon Steel & Sumitomo Metal Technical Report*, September, No 110: 90–96
- Kimura T, Sumi H, Kitani Y (2005) High strength steel plates and welding consumables for architectural construction with excellent toughness in welded joint-“JFE EWEL” technology for excellent quality in HAZ of high heat input welded joints. *JFE Technical Report*, March, No 5: 45–52
- Bailey N (1991) Submerged arc welding ferritic steels with alloyed metal powders. *Weld J* 70(8):187s–206s
- Ryu K-M, Kim D-W, Lee J-W, Bang H-C, Park C-K, Jeong H (2017) High heat input electro-gas welding of TMCP plate for steel storage tanks. *J Weld Join* 35(6):27–31 (in Korean)
- Fleck NA, Grong O, Edward GR, Matlock DK (1986) The role of filler metal wire and flux composition in submerged arc weld metal transformation kinetics. *Weld J* 65(5):113s–128s
- Kitani Y, Ikeda R, Ono M, Ikeuchi K (2009) Improvement of weld metal toughness in high heat input electro-slag welding of low carbon steel. *Weld World* 53(3/4):57–63
- Svensson L-E, Grefott B (1990) Microstructure and impact toughness of C-Mn weld metals. *Weld J* 89(12):454s–461s
- Evans GM (1992) The effect of titanium in SMA C-Mn steel multipass deposits. *Weld J* 71(12):447s–454s
- Evans GM (1996) Microstructure and properties of ferritic steel welds containing Ti and B. *Weld J* 75(8):251s–260s
- Kluken AO, Grong O (1989) Structure property relationships in reheated SA steel weld metals. *Trends in Weld Res, Proc. of 2nd Int. Conf.*, May 14–18, Gatlinburg, TN, USA, pp. 781–786
- Cerjak H, Letofsky E, Pitoiset X, Seiringer A (1995) The effect of microstructure on the toughness of C-Mn multirun weld deposit. *Trends in Weld Res, Proc. of 4th Int. Conf.*, June 5–6, Gatlinburg, TN, USA, pp. 535–540
- Song HY, Zhang W, Babu SS, Feng Z (2012) Toward understanding of mechanical property degradation of steel welds in high-pressure hydrogen transmission pipeline-role of microstructure. *Trends in Weld Res, Proc. of 9th Int. Conf.*, June 4–8, Chicago, Illinois, USA, pp. 461–468
- Song HY, Evans GM, Babu SS (2014) Effect of microstructural heterogeneities on scatter of toughness in multi-pass weld metal of C-Mn steels. *Sci Technol Weld Join* 19(5):376–384
- Kang Y, Park G, Jeong S, Lee C (2017) Microstructure and mechanical properties of reheated zones in the multi-pass weld metal of high-strength steel. *J Weld Join* 35(6):21–26 (in Korean)
- Munnig Schmidt-van der Gurg MA, Hoekstra S, Den Ouden G (1985) Influence of microstructure on mechanical properties of two single-bead ferritic weld metals. *Weld J* 64(3):63s–70s
- Terashima H, Hart PHM (1984) Effect of aluminum on C-Mn-Nb steel submerged arc weld metal properties. *Weld J* 60(6):173s–183s
- Norcross JE (1965) Electroslag/electro-gas welding in the free world. *Weld J* 44(3):177–196
- Kearns WH (ed) (1978) *Welding Handbook*, 7th edn. Miami, p 254
- Culp JD (1979) Electroslag weldments: performance and needed research. *Weld J* 58(7):27–41
- Devletian JH, Singh D, Turpin RB (1997) Electroslag welding of an advanced double-hull design ship. *Weld J* 76(8):49–52
- Choi W-H, Cho S-K, Choi W-K, Ko S-G, Han J-M (2012) Effects of microstructures on the toughness of high heat input EG welded joint of EH36-TM steel. *J KWJS* 30(1):64–71 (in Korean)
- Seo K, Ryoo H, Kim HJ, Park C, Lee C (2020) Local variation of impact toughness in tandem electro-gas welded joint. *Weld World* 64(3):457–465
- Shiliang W, Weiping H, Bogang T (1987) Improving the toughness of weld metal by adding rare earth elements. *Weld Int* 1(3):284–287
- Chen JH, Yan C (1988) Fracture behavior of C-Mn steel multipass MMA weld metals at -60°C in Charpy V testing. *Mater Sci Technol* 4(8):732–739
- Hughes RK, Ritter JC (1995) Cleavage fracture properties of high strength steel weldments. *Trends in Weld Research, Proceed. of 7th Int. Conf.*, 5–8 June Gatlinburg, TN, USA, pp. 645–650

31. Kojima A, Kasuya T, Tsuruta T, Minami K (2007) Study on application of electrogas arc welding to SM570 steel in bridge fabrication. *Trans Jpn Soc Cevil Eng A* 63(1):1–13 (in Japanese)
32. IACS UR W-11: Normal and higher strength hull structural steels, Rev. 9, May 2017, London, UK
33. A516/A516M-10 (2015) Standard specification for pressure vessel plates, carbon steel, for moderate and lower-temperature service, ASTM, USA
34. AWS A5.26/A5.26M-97 (2009) Specification for carbon and low-alloy steel electrodes for electro-gas welding. AWS, Miami
35. Komizo Y, Punshon CS, Gooch TG, Blakeley PJ (1986) Effects of process parameters on centerline solidification in EB welds. *Metal Const* 18(2):104R–111R

**Publisher's note** Springer Nature remains neutral with regard to jurisdictional claims in published maps and institutional affiliations.